Elastic Instability behind Brittle Fracture

D. Riccobelli,[1] P. Ciarletta,[1] G. Vitale,[2] C. Maurini,[3] and L. Truskinovsky[4,*]
[1]*MOX—Dipartimento di Matematica, Politecnico di Milano, 20133 Milano, Italy*
[2]*Laboratoire de Mecanique des Solides, École Polytechnique, 91128 Palaiseau, France*
[3]*CNRS, Institut Jean Le Rond d'Alembert, Sorbonne Université, UMR 7190, 75005 Paris, France*
[4]*ESPCI ParisTech, PMMH, CNRS—UMR 7636, 75005 Paris, France*

(Received 14 November 2023; revised 12 April 2024; accepted 6 May 2024; published 13 June 2024)

We argue that nucleation of brittle cracks in initially flawless soft elastic solids is preceded by a nonlinear elastic instability, which cannot be captured without accounting for geometrically precise description of finite elastic deformation. As a prototypical problem we consider a homogeneous elastic body subjected to tension and assume that it is weakened by the presence of a free surface which then serves as a location of cracks nucleation. We show that in this maximally simplified setting, brittle fracture emerges from a symmetry breaking elastic instability activated by softening and involving large elastic rotations. The implied bifurcation of the homogeneous elastic equilibrium is highly unconventional for nonlinear elasticity as it exhibits strong sensitivity to geometry, reminiscent of the transition to turbulence in fluids. We trace the postbifurcational development of this instability beyond the limits of applicability of scale-free continuum elasticity and use a phase-field approach to capture the scale dependent subcontinuum strain localization, signaling the formation of actual cracks.

DOI: 10.1103/PhysRevLett.132.248202

While linearized elasticity theory is usually sufficient in problems involving propagation of preexisting cracks [1–3], we present evidence that, at least for some classes of soft materials, the description of crack nucleation requires an account of both geometric and physical elastic nonlinearities [4,5]. To elucidate the physical origin of the failure of linear theory, we build a continuous path from surface instability in tension to fracture.

The phenomenon of surface fracture is of considerable recent interest because the submicron parts employed in many modern applications are effectively defect-free and their fracture usually originates on unconstrained external surfaces [6]. Crack nucleation at the surface is also of importance for the understanding of the fragmentation of various brittle surface layers [7–10]. More generally, the emergence of surface fracture patterns [11,12] is an example of a symmetry breaking instability which is at the heart of complexity development in soft matter physics [13,14] and biophysics [15,16].

Nonlinear elastic instabilities were studied extensively in the context of compressive buckling [17–25]. Elastic instabilities can also take place under tension, with necking, wrinkling, and shear banding, as the most prominent examples [26–30]. However, the potential relation of tensile instabilities to fracture has been largely overlooked. Several studies attempted to develop conceptual links between the bulk crack nucleation and material softening and used them to advance various phenomenological nucleation criteria [11,31–38]. Still, an understanding of how such criteria relate to the subtle interplay between geometric and physical nonlinearities along the crack nucleation path remains obscure.

Brittle cracking of soft solids is not uncommon, as it is exemplified by an abrupt failure of an elastic rubber band under tension. In particular, brittle-soft behavior is characteristic for hydrogels [39–42], where the diverging stress at the crack tip is typically accompanied not only by large stretches but also by large rotations and several candidate mechanisms are debated as potential regulators of the underlying material failure at the microscale [43].

In this Letter we use the geometrically simplest setting to explore both linear and nonlinear stages of the tensile instability in a soft solid which culminates in the formation of a brittle crack. The implied instability is of spinodal type [39–41] but with a peculiarity that it is associated with the *surface* rather than with the *bulk* [42–46]. The degenerate nature of this instability in the purely elastic setting [47] leads to a high sensitivity of the emerging patterns to sample geometry. Such sensitivity is typical for nonlinear systems without an internal length scale and the ensuing crack nucleation scenario is reminiscent, for instance, of a transition to turbulence. Regularization of the problem, bringing a fixed internal length scale, naturally simplifies the picture, as it is already known from the study of the prototypical one-dimensional models [48,49].

Our first goal is to show in detail how the elastic instability serves as a precursor of the ultimate strain localization. Then, since the emerging strain singularity renders the continuum elasticity inadequate, the modeling paradigm is changed and the goal now is to capture the

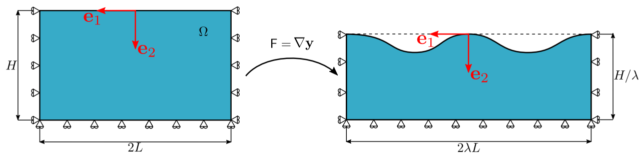

FIG. 1. Schematic representation of the considered surface instability showing the reference and the actual configurations, while also detailing the nature of the boundary conditions.

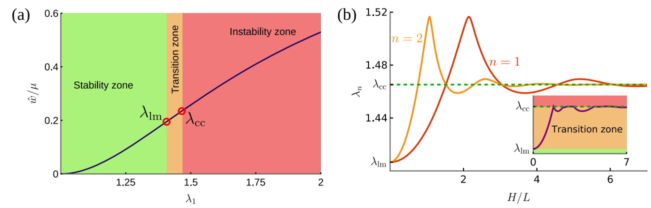

FIG. 2. (a) The energy density $\hat{w}(\lambda)$ of our softening material as a function of the maximal principal stretch λ_1. (b) The stability curves for the two modes with $n = 1$, 2; the purple line in the inset represents the function $\lambda_{\rm cr}(H/L)$.

formation of sharp cracks. To describe the role of microscales in such a sharpening process we resort to a phase-field-type extension of the continuum theory [34,48,50,51]. We show that such a hybrid approach allows one to model seamlessly the whole process from a continuum elastic instability to a subcontinuum evolution of developed cracks.

Consider a 2D rectangular body $\Omega = [-L, L] \times [0, H]$. Denote by $\mathbf{x} \in \Omega$ points in the reference configuration and by $\mathbf{y}(\mathbf{x})$ their deformed positions, see Fig. 1. Working directly with the deformation gradient $\mathsf{F} = \nabla \mathbf{y}$ we account for geometric nonlinearities. In such an approach, not only the principal stretches $\lambda_{1,2}$ (the square roots of the eigenvalues of $\mathsf{F}^T\mathsf{F}$) can be large, but also the description of rotations is geometrically exact [18].

Assume that the material is incompressible, so that $\det \mathsf{F} = \lambda_1\lambda_2 = 1$, and isotropic, so that the elastic energy density can be written as $\hat{w}(\lambda_1) = w(\lambda_1, \lambda_1^{-1})$. We can then write the force balance in the form $\nabla \cdot \mathsf{P} = 0$, where P_{ij} are the components of the first Piola-Kirchhoff stress tensor $\mathsf{P} = \partial w/\partial \mathsf{F} + p\mathsf{F}^{-1}$ and p is the Lagrange multiplier enforcing the incompressibility constraint.

Suppose further that the body Ω is loaded in a two-sided hard device, such that $y_1 = \lambda x_1$ at $x_1 = \pm L$, where λ is the applied stretch which serves as the control parameter. Then on the side boundaries (at $x_1 = \pm L$) the horizontal displacements are prescribed $y_1 = \pm\lambda L$ while the possibility of free sliding is ensured by the second condition $P_{12} = 0$. The upper boundary $x_2 = 0$ will be kept free so that $P_{22} = P_{21} = 0$ while the lower boundary $x_2 = H$ will be constrained only partially so that $y_2 = H/\lambda$ and $P_{21} = 0$. The ensuing basic problem of elasticity theory admits a homogeneous solution $\mathbf{y}^{(\mathbf{0})} \coloneqq \mathsf{F}^{(\mathbf{0})}\mathbf{x}$, where $\mathsf{F}^{(0)} = \mathrm{diag}(\lambda, \lambda^{-1})$; the corresponding pressure is $p^{(0)} \coloneqq -\lambda^{-1}\partial w/\partial \lambda_2$.

To study the stability of this solution, we use standard methods [20,52–54] and write the perturbed displacement and pressure fields, in the form $\mathbf{y} = \mathbf{y}^{(0)} + \sum_{j=1}^{\infty} \varepsilon^j \mathbf{u}^{(j)}$ and $p = p^{(0)} + \sum_{j=1}^{\infty} \varepsilon^j p^{(j)}$ where ε is a small parameter. Inserting these expansions in the force balance equation we obtain, at the first order, a linear boundary value problem for $\mathbf{u}^{(1)}$ and $p^{(1)}$.

To illustrate the results we introduce the stream function $\mathbf{u}^{(1)}(\mathbf{x}) = (\partial_{\mathbf{2}}\chi, -\partial_{\mathbf{1}}\chi)$, and write the solution of the first order equilibrium problem in the form $\chi = iAg(\gamma x_2)\exp(i\gamma x_1)/\gamma + \mathrm{c.c.}$, where A is still undefined complex amplitude and c.c. denotes complex conjugate. Here we have also introduced the horizontal wave number $\gamma = (n\pi)/(2\lambda L)$, where n is an integer with even (odd) values representing symmetric (asymmetric) modes, respectively. The expression for $p^{(1)}(\mathbf{x})$ in terms of $g(\gamma x_2)$ is too long to be presented here, see Ref. [55].

Following closely [20], we write the real valued function g in the form $g(\gamma x_2) = \sum_{k=1}^{4} C_k \exp[\gamma\omega_k x_2]$, where $\omega_1 = -\omega_2 = \alpha$, $\omega_3 = -\omega_4 = \beta$. The constants α, β can be found from the relations $\alpha\beta = \lambda^2$ and $\alpha^2 + \beta^2 + 2 = \lambda(\lambda^4 - 1)\eta$; the elastic energy enters these relations through the function $\eta(\lambda) = \hat{w}''(\lambda)/\hat{w}'(\lambda)$ which characterizes the physical nonlinearity.

The bifurcation points $\lambda_n(H/L)$, parametrized by the integers $n(H/L)$, can be found from the condition that there exists a nontrivial set of coefficients C_k, such that the functions $\mathbf{u}^{(1)}$ and $p^{(1)}$ satisfy the boundary conditions at the linear order. This gives an explicit nonlinear algebraic equation, see Ref. [55]. We can then define $\lambda_{\rm cr}(H/L) = \min_{n\geq 1}\lambda_n(H/L)$ and denote by $n_{\rm cr}(H/L)$ the corresponding critical mode. To illustrate the sensitivity of the instability threshold $\lambda_{\rm cr}(H/L)$ to the geometry of the domain characterized by the ratio H/L, we need to choose a specific energy density.

To account for strain softening in the simplest form, we assume that $w = \mu(I-2)/I$, where $I = \lambda_1^2 + \lambda_2^2$ is the first strain invariant and μ is the measure of rigidity (see more about this particular choice in [55]). In this case $\hat{w}(\lambda) = \mu(\lambda^2 - 1)^2/[2(\lambda^4 + 1)]$ and the softening ($\hat{w}'' < 0$) takes place for $\lambda > \lambda_{\rm lm} = \sqrt[4]{(1/3)(\sqrt{33} + 6)}$, see Fig. 2(a) and [55]. The value $\lambda_{\rm lm}$ is known as the Considère or the load maximum (LM) threshold [54,62,63], where by the "load" we understand the axial stress in the direction of traction $P(\lambda) = \mathbf{e}_1 \cdot \mathsf{P} \cdot \mathbf{e}_1 = \hat{w}'(\lambda)$; reaching this threshold indicates the occurrence of necking in slender bodies [20,26,64,65]. It can be also shown that crossing the LM threshold is a necessary condition for the occurrence of a generic elastic instability [20].

Observe next that, independently of the value of n, the functions $\lambda_n(H/L)$, shown in Fig. 2(b) for $n = 1$, 2, approach the point $\lambda_{\rm lm} \simeq 1.407$ in the limit of infinitely small aspect ratios ($H \ll L$, thin domains) and the point

$\lambda_{cc} \simeq 1.465$ in the limit of infinitely large aspect ratios ($H \gg L$, thick domains).

The emerging threshold λ_{cc} indicates the failure of the complementing condition (CC) [44,46,66–68]. In an infinite system it marks the onset of wrinkling instability with all wave numbers becoming unstable simultaneously. In our case the value of the CC threshold can be found analytically as a solution of the transcendental equation $\eta(\lambda_{cc}) = -\lambda_{cc}^{-3}$ [55]. Note that in the classical geometrically linearized elasticity theory, where both stretches and rotations are small and therefore we can use the approximation $w(\mathsf{E})$ with $\mathsf{E} = (1/2)(\nabla\mathbf{u} + \nabla\mathbf{u}^T)$, the very difference between the thresholds λ_{cc} and λ_{lm} disappears and the whole complexity of the emerging stability diagram is lost [55].

Outside these two limits (of infinitely thin and infinitely thick domains), the behavior of the function $\lambda_{cr}(H/L)$ looks uncorrelated. However, a remarkable underlying structure reveals itself if we focus instead on the integer valued function $n_{cr}(H/L)$, see Fig. 3.

First of all, we observe that the necking-type instability with $n_{cr} = 1$ is not a feature of slender bodies only, but appears periodically as one changes the aspect ratio. Similarly, the wrinkling-type instability with $n_{cr} = \infty$ appears at periodically distributed values of the aspect ratio. In both cases the period is the same and is equal to $\Delta(H/L) = 4\lambda_{cc}^3/\sqrt{-1 + 2\lambda_{cc}^2 + 3\lambda_{cc}^4}$, see Ref. [55] for details.

Overall, we observe a periodic distribution of "staircase" structures with an infinite number of steps in every period representing all integer values of n_{cr} from necking with $n_{cr} = 1$ to wrinkling with $n_{cr} = \infty$. Each of these staircases demonstrates the same "devilish" features with step accumulation taking place around the recurrent wrinkling thresholds (where the unstable mode becomes singularly localized near the free surface). In other words, each staircase describes a crossover between necking and wrinkling with the steps emerging due to the locking in the parameter intervals where horizontal and vertical oscillations of the displacement field are resonant with the domain geometry. To the best of our knowledge, the reported extreme sensitivity of the critical wave number to the aspect ratio and the emergence of special geometries where the instability pattern changes dramatically from fully localized to fully delocalized, have not been previously observed in nonlinear elasticity problems.

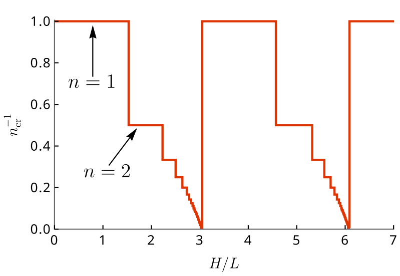

FIG. 3. The inverse of the critical mode n_{cr} versus the aspect ratio H/L. The accumulation points correspond to $n = \infty$.

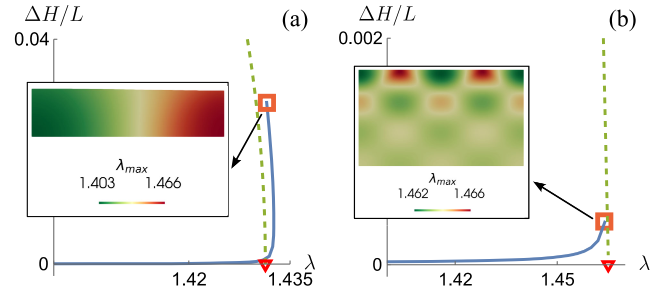

FIG. 4. Bifurcation diagrams showing the amplitude ΔH of the unstable mode on the free surface for the cases: (a) $H/L = 1$ (near necking case) and (b) $H/L = 2.5$ (near wrinkling case). The red triangles denote the critical thresholds λ_{cr}. Solid and dashed lines represent the results of the finite element simulations and of the weakly nonlinear analysis, respectively. Insets show the distribution of the maximal principal stretch λ_{max} in the actual configuration corresponding to the location of the square marker.

The revealed distribution of the stability thresholds can be corroborated analytically using the observation that for $H/L \gg 1$ (when $\lambda_{cr} \sim \lambda_{cc}$) one can approximate the actual problem of finding $n_{cr}(H/L)$, involving minimization of an implicitly given function over a discrete set, by a model problem $N = \arg\ \max_\xi[\sin(a\xi)/e^\xi]$, where ξ is a positive integer and $a \sim H/L$. The model problem can be solved explicitly and its solution N can be formally proved to exhibit the periodic staircase structure of the type shown in Fig. 3, see Ref. [55] for details.

To determine the nature of detected bifurcations, we now perform a standard weakly nonlinear amplitude expansion [4,69–75]. The idea is to compute the next terms of the perturbative expansion $\mathbf{u}^{(2)}$, $p^{(2)}$ and use the obtained information to determine λ dependence of the amplitude A near the bifurcation point λ_{cr}. In this respect the "near necking" (single-mode instability) and the "near wrinkling" (multimode instability) regimes function differently.

Indeed, in the more conventional near necking regimes, where the buckling thresholds λ_n are well separated and only a finite number of modes are initially activated in the postbuckling regime, the natural small parameter is known to be $\varepsilon = \sqrt{|\lambda - \lambda_{cr}|/\lambda_{cr}}$. By expanding the energy functional $\mathcal{W} = \int_\Omega w\, d\mathbf{x}$ in ε we obtain [55] $\Delta\mathcal{W} = \varepsilon^4(\theta_2|A|^2 + \theta_4|A|^4) + o(\varepsilon^4)$, where $\theta_2(\lambda)$, $\theta_4(\lambda)$ are known real functions. The requirement of stationarity of the energy in A (at order ε^4), gives the expression for the amplitude $A = \sqrt{-\theta_2/(2\theta_4)}$ where θ_2 and θ_4 have the same sign. This characterizes the bifurcation as a subcritical (unstable) pitchfork, see the dashed line in Fig. 4(a). The implied unstable postbuckling regime is the diffuse necking illustrated in the inset in Fig. 4(a).

The near wrinkling regimes, where buckling thresholds accumulate, are markedly different. In this case a small increment of the control parameter λ away from the critical value λ_{cr} activates an essentially infinite number of instability modes. Therefore in the weakly nonlinear approximation an unstable mode interacts with many other modes. The availability of a broad bandwidth of such modes requires a different scaling and one can show that the natural small parameter in this case is $\varepsilon = |\lambda - \lambda_{\mathrm{cr}}|/\lambda_{\mathrm{cr}}$, see Refs. [76,77] for similar analyses. To take into account all the implied interactions we need to modify the expression for the first order stream function adopted in the near necking case and write instead $\chi = \sum_{m=-\infty}^{+\infty} i(A_m/\gamma m) g(\gamma m x_2) \exp(i\gamma m x_1) +$ c.c. where m is an integer and A_m is amplitude of the mode m. We can then proceed as before and find the amplitude equation, accounting for cubic resonances, which now takes the form of an infinite system: $\theta_1 A_m + \sum_{k=-\infty}^{+\infty} \theta_{3(k)} A_k A_{m-k} = 0$. Here again the real functions $\theta_1(\lambda; m)$ and $\theta_{3(k)}(\lambda; m)$ are known explicitly [55]. The analysis shows that the bifurcation is again a subcritical pitchfork, see the dashed line in Fig. 4(b), which implies that the incipient postbifurcational mode, illustrated in the inset in Fig. 4(b), is again unstable.

To complement this analytical study we also performed some direct numerical simulations. For numerical convenience we slightly modified the model by introducing into our original energy density $w(\mathsf{F})$ a dependence on $J = \lambda_1 \lambda_2$, a measure of volumetric deformation. More specifically we used the expression $w_J(\mathsf{F}) = (\mu/I)(I - 2\log J - 2) + (\Lambda/2)(\log J)^2$ with Λ equal to 100μ which corresponds to almost incompressibility; note that at $\Lambda \to +\infty$ we recover the original model.

The bifurcated branch was obtained after we introduced an imperfection on the free boundary with a wave number of the instability mode and a small amplitude of the order of $10^{-5}L$, see the blue lines in Figs. 4(a) and 4(b). We used an arclength continuation method [78,79] which allowed us to reach the state of strain focusing causing local violation of the complementing condition. The deformation patterns at such limits (of the applicability of continuum elasticity) are illustrated in the insets in Figs. 4(a) and 4(b) for the typical near necking and near wrinkling regimes.

The ultimate strain localization, which induced the break down of our continuum model, is indicative of the trend towards the formation of atomically sharp cracks. To capture the latter, the scale-free continuum theory, which is expected to be operative only on long waves, can be regularized through the introduction of a subcontinuum length scale. A convenient approach of this type is a phase-field model of fracture, e.g., [50,51,80,81]. Specifically, we assume that

$$w_{\mathrm{pf}}(\mathsf{F}, \alpha) = (1-\alpha)^2(\mu/2)(I-2) + \mu\alpha^2 + \mu\ell_0^2\|\nabla\alpha\|^2,$$

where $\alpha(\mathbf{x}) \in [0,1]$ is a subcontinuum damagelike scalar field: the compatibility with our original nonlinear

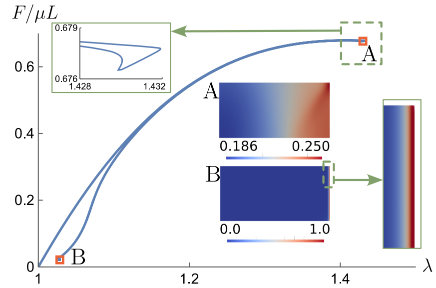

FIG. 5. Normalized axial force $F/\mu L$ versus the mean stretch λ for the near necking case ($H/L = 1$). The insets on the right show the distribution of the internal variable α in the reference configuration corresponding to the points A and B. The parameter $\ell_0/H = 0.01$.

elasticity model is ensured by the fact that $w(\mathsf{F}) = \min_{\alpha\in[0,1]}[(1-\alpha)^2(\mu/2)(I-2) + \mu\alpha^2]$. The regularization is achieved through the term penalizing gradients of α which brings an internal length scale ℓ_0. At $\ell_0 \ll L$ this approach is known to be equivalent to the Griffith fracture model with the toughness $G_c = \mu\ell_0/2$ [34,50,82].

Moving in this way beyond continuum elasticity and adopting again the weak compressibility regularization, we performed a series of numerical simulations with the goal to capture the actual formation of cracks. We used a Newton's algorithm complemented by a standard pseudo-arclength continuation technique [78] to minimize (at each value of the loading parameter λ) the energy with respect to both, the deformation field $\mathbf{y}(\mathbf{x})$, and the auxiliary scalar field $\alpha(\mathbf{x})$.

The results of the two representative numerical simulations, illustrating qualitatively different near necking and near wrinkling regimes, are presented in Figs. 5 and 6. In both figures the (unstable) postbifurcational response is represented through the dimensionless force-stretch relation $F(\lambda) = \int_{-H}^{0} P_{11}(\lambda)|_{x_1=L} dx_2$. The deformed configurations close and far from the bifurcation points are shown in the insets. Note that while in near wrinkling regime we show for simplicity only the case with two emerging

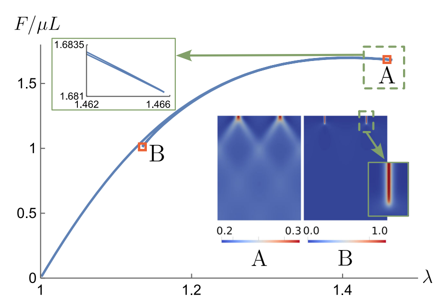

FIG. 6. Normalized axial force $F/\mu L$ versus the mean stretch λ for the near wrinkling case ($H/L = 2.5$). The insets on the right show the distribution of the internal variable α in the reference configuration corresponding to the points A and B. The parameter $\ell_0/H = 0.01$.

cracks, the aspect ratio of the domain and the regularization length could be chosen differently to obtain arbitrary many cracks.

The common feature of the two cases, shown in Figs. 5 and 6, is the gradual sharpening of the initially diffuse local "nonaffinity" measured by parameter α. The actual formation of cracks can be linked to the moment of reaching the value $\alpha \sim 1$ inside the localized regions with the thickness of order of subcontinuum scale ℓ_0. Since the focus of our Letter is crack nucleation, we did not advance our simulations till the complete break down of the slab which is preceded by secondary bifurcations representing both crack branching and crack arrest [11]. Overall, the presence in this problem of a subcritical bifurcation indicates the possibility of abrupt (dynamic) transition from a homogeneous state to a cracked state which is a typical scenario in brittle fracture.

To conclude, using the simplest geometrical setting and focusing on initially flawless soft solids, we showed that crack nucleation is preceded by an elastic instability which can be identified using continuum elasticity theory only if the latter accounts properly for both geometrical and physical nonlinearities. Such elasticity theory predicts a surprisingly complex linear stability diagram with recurrent geometry-sensitive crossovers between necking and wrinkling modes. Both necking and wrinkling instabilities were shown to evolve towards the formation of developed cracks when the classical elasticity was seamlessly extended as a phase-field type model. Our analysis builds a bridge between nonlinear elasticity and fracture mechanics and points to the existence of purely elastic precursors of crack nucleation. Similar mechanisms should be operative in other highly nonlinear manifestations of elasticity such as cavitation [83,84], phase nucleation [85,86], and creasing [87,88].

D. R. and P. C. gratefully acknowledge partial support from grant Dipartimento di Eccellenza 2023-2027 and MIUR, PRIN 2017 Project "Mathematics of active materials: From mechanobiology to smart devices." D. R. has been partially supported by MIUR, PRIN 2022 Project "Mathematical models for viscoelastic biological matter," 202249PF73. D. R. and P. C. are members of the INdAM research group GNFM. L. T. acknowledges the support from the French Grant No. ANR-10-IDEX-0001-02 PSL. This work was performed using HPC resources from GENCI-IDRIS (Grant No. 2023-AD010913451R1).

[*]lev.truskinovsky@espci.fr

[1] L. D. Landau, E. M. Lifshitz, A. M. Kosevich, and L. P. Pitaevskii, *Theory of Elasticity: Volume 7* (Elsevier, New York, 1986), Vol. 7.
[2] D. Broek, *The Practical Use of Fracture Mechanics* (Springer Science & Business Media, New York, 2012).
[3] K. B. Broberg, *Cracks and Fracture* (Elsevier, New York, 1999).
[4] S. S. Antman, *Nonlinear Problems of Elasticity* (Springer, New York, 2005), pp. 513–584.
[5] J. M. Marsden and T. J. R. Hughes, *Mathematical Foundations of Elasticity* (Prentice-Hall Inc., New York, 1983).
[6] G. Dehm, B. N. Jaya, R. Raghavan, and C. Kirchlechner, Acta Mater. **142**, 248 (2018).
[7] J. W. Hutchinson and Z. Suo, Adv. Appl. Mech. **29**, 63 (1991).
[8] H. Colina, L. de Arcangelis, and S. Roux, Phys. Rev. B **48**, 3666 (1993).
[9] U. A. Handge, Y. Leterrier, G. Rochat, I. M. Sokolov, and A. Blumen, Phys. Rev. E **62**, 7807 (2000).
[10] H. Alarcón, O. Ramos, L. Vanel, F. Vittoz, F. Melo, and J.-C. Géminard, Phys. Rev. Lett. **105**, 208001 (2010).
[11] B. Bourdin, J.-J. Marigo, C. Maurini, and P. Sicsic, Phys. Rev. Lett. **112**, 014301 (2014).
[12] L. Truskinovsky, G. Vitale, and T. Smit, Int. J. Eng. Sci. **83**, 124 (2014).
[13] J. Kim, J. Yoon, and R. C. Hayward, Nat. Mater. **9**, 159 (2010).
[14] E. Hohlfeld and L. Mahadevan, Phys. Rev. Lett. **106**, 105702 (2011).
[15] M. B. Amar and A. Goriely, J. Mech. Phys. Solids **53**, 2284 (2005).
[16] P. Ciarletta, V. Balbi, and E. Kuhl, Phys. Rev. Lett. **113**, 248101 (2014).
[17] M. A. Biot, *Mechanics of Incremental Deformations* (John Wiley & Sons, New York, 1965).
[18] R. W. Ogden, *Non-Linear Elastic Deformations* (Dover, New York, 1984).
[19] D. Bigoni, *Nonlinear Solid Mechanics: Bifurcation Theory and Material Instability* (Cambridge University Press, Cambridge, England, 2012).
[20] R. Hill and J. Hutchinson, J. Mech. Phys. Solids **23**, 239 (1975).
[21] G. DelPiero and R. Rizzoni, J. Elast. **93**, 203 (2008).
[22] J. Sivalogathan and S. J. Spector, Proc. R. Soc. A: Math. Phys. Eng. Sci. **466**, 1167 (2010).
[23] Y. Grabovsky and L. Truskinovsky, Continuum Mech. Thermodyn. **19**, 211 (2007).
[24] K. Sawyers and R. Rivlin, J. Elast. **12**, 101 (1982).
[25] N. Triantafyllidis, W. M. Scherzinger, and H.-J. Huang, Int. J. Solids Struct. **44**, 3700 (2007).
[26] B. Audoly and J. W. Hutchinson, J. Mech. Phys. Solids **97**, 68 (2016).
[27] Q. Li and T. J. Healey, J. Mech. Phys. Solids **97**, 260 (2016).
[28] E. Cerda and L. Mahadevan, Phys. Rev. Lett. **90**, 074302 (2003).
[29] J. W. Hutchinson and V. Tvergaard, Int. J. Solids Struct. **17**, 451 (1981).
[30] R. Hill and J. Hutchinson, J. Mech. Phys. Solids **23**, 239 (1975).
[31] P. Klein and H. Gao, Eng. Fract. Mech. **61**, 21 (1998).
[32] S. A. Silling, O. Weckner, E. Askari, and F. Bobaru, Int. J. Fract. **162**, 219 (2010).
[33] A. Shekhawat, S. Zapperi, and J. P. Sethna, Phys. Rev. Lett. **110**, 185505 (2013).
[34] E. Tanné, T. Li, B. Bourdin, J.-J. Marigo, and C. Maurini, J. Mech. Phys. Solids **110**, 80 (2018).
[35] A. Kumar, B. Bourdin, G. A. Francfort, and O. Lopez-Pamies, J. Mech. Phys. Solids **142**, 104027 (2020).

[36] P. K. Kristensen, C. F. Niordson, and E. Martínez-Pañeda, Phil. Trans. R. Soc. A **379**, 20210021 (2021).
[37] T. Hao and Z. M. Hossain, Phys. Rev. B **100**, 014204 (2019).
[38] C. J. Larsen, Mech. Res. Commun. **128**, 104059 (2023).
[39] C. J. Gagne, H. Gould, W. Klein, T. Lookman, and A. Saxena, Phys. Rev. Lett. **95**, 095701 (2005).
[40] A. O. Schweiger, K. Barros, and W. Klein, Phys. Rev. E **75**, 031102 (2007).
[41] W. Klein, T. Lookman, A. Saxena, and D. M. Hatch, Phys. Rev. Lett. **88**, 085701 (2002).
[42] H. C. Simpson and S. J. Spector, J. Elast. **15**, 229 (1985).
[43] A. Benallal, R. Billardon, and G. Geymonat, in *Bifurcation and Stability of Dissipative Systems* (Springer, New York, 1993), pp. 1–44.
[44] H. C. Simpson, J. Elast. **139**, 1 (2020).
[45] A. Mielke and P. Sprenger, J. Elast. **51**, 23 (1998).
[46] P. V. Negrón-Marrero and E. Montes-Pizarro, J. Elast. **107**, 151 (2012).
[47] S. G. Mikhlin, Russ. Math. Surv. **28**, 45 (1973).
[48] O. U. Salman and L. Truskinovsky, J. Mech. Phys. Solids **154**, 104517 (2021).
[49] A. Gupta and T. J. Healey, J. Elast. 1 (2023) 10.1007/s10659-023-10019-8.
[50] B. Bourdin, G. Francfort, and J.-J. Marigo, J. Mech. Phys. Solids **48**, 797 (2000).
[51] A. Karma, D. A. Kessler, and H. Levine, Phys. Rev. Lett. **87**, 045501 (2001).
[52] Y. Cao and J. W. Hutchinson, Proc. R. Soc. A **468**, 94 (2012).
[53] M. A. Holland, B. Li, X. Q. Feng, and E. Kuhl, J. Mech. Phys. Solids **98**, 350 (2017).
[54] J. Li, H. Varner, and T. Cohen, J. Mech. Phys. Solids **172**, 105171 (2023).
[55] See Supplemental Material at http://link.aps.org/supplemental/10.1103/PhysRevLett.132.248202 for the details of the computations, which includes Refs. [56–61].
[56] F. Charru, *Hydrodynamic Instabilities* (Cambridge University Press, Cambridge, England, 2011), Vol. 37.
[57] Y. B. Fu and P. Ciarletta, Proc. R. Soc. A **471**, 20140979 (2015).
[58] M. Alnæs, J. Blechta, J. Hake, A. Johansson, B. Kehlet, A. Logg, C. Richardson, J. Ring, M. E. Rognes, and G. N. Wells, Arch. Num. Software **3**, 9 (2015).
[59] D. Riccobelli, G. Noselli, and A. DeSimone, Proc. R. Soc. A **477**, 20200817 (2021).
[60] S. Balay, S. Abhyankar, M. Adams, P. Brune, K. Buschelman, L. Dalcin, W. Gropp, B. Smith, D. Karpeyev, D. Kaushik *et al.*, Petsc users manual revision 3.7, Technical Report, Argonne National Lab.(ANL), Argonne, IL, United States, 2016.
[61] P. Chadwick and R. W. Ogden, Arch. Ration. Mech. Anal. **44**, 54 (1971).
[62] I. S. Yasnikov, A. Vinogradov, and Y. Estrin, Scr. Mater. **76**, 37 (2014).
[63] S. M. Fielding, Phys. Rev. Lett. **107**, 258301 (2011).
[64] V. Tvergaard, Comput. Methods Appl. Mech. Eng. **103**, 273 (1993).
[65] A. Needleman, Mech. Mater. **116**, 180 (2018).
[66] M. Šilhavý, *The Mechanics and Thermodynamics of Continuous Media* (Springer, Berlin Heidelberg, 1997).
[67] X. Liu and B.-W. Schulze, *Boundary Value Problems with Global Projection Conditions* (Springer, New York, 2018), Vol. 265.
[68] M. A. Biot, Appl. Sci. Res. **12**, 168 (1963).
[69] P. Becherer, A. N. Morozov, and W. van Saarloos, Physica (Amsterdam) **238D**, 1827 (2009).
[70] M. Weinstein, Proc. R. Soc. A **375**, 155 (1981).
[71] B. Audoly, Phys. Rev. E **84**, 011605 (2011).
[72] Y. Pomeau, S. Zaleski, and P. Manneville, Phys. Rev. A **27**, 2710 (1983).
[73] W. T. Koiter, *On the Stability of Elastic Equilibrium* (National Aeronautics and Space Administration, Dayton, Ohio, 1967).
[74] B. Budiansky, Adv. Appl. Mech. **14**, 1 (1974).
[75] *W. T. Koiter's Elastic Stability of Solids and Structures*, edited by A. M. A. van der Heijden (Cambridge University Press, Cambridge, England, 2008).
[76] Y. B. Fu and R. W. Ogden, Continuum Mech. Thermodyn. **11**, 141 (1999).
[77] P. Ciarletta and Y. Fu, Int. J. Nonlinear Mech. **75**, 38 (2015).
[78] R. Seydel, *Practical Bifurcation and Stability Analysis* (Springer Science & Business Media, New York, 2009), Vol. 5.
[79] Y. Su, D. Riccobelli, Y. Chen, W. Chen, and P. Ciarletta, Proc. R. Soc. A **479**, 20230358 (2023).
[80] I. S. Aranson, V. A. Kalatsky, and V. M. Vinokur, Phys. Rev. Lett. **85**, 118 (2000).
[81] L. O. Eastgate, J. P. Sethna, M. Rauscher, T. Cretegny, C.-S. Chen, and C. R. Myers, Phys. Rev. E **65**, 036117 (2002).
[82] A. A. Griffith, Phil. Trans. R. Soc. A **221**, 163 (1921).
[83] J. M. Ball, Phil. Trans. R. Soc. A **306**, 557 (1982).
[84] A. Kumar and O. Lopez-Pamies, J. Mech. Phys. Solids **150**, 104359 (2021).
[85] T. J. Healey and U. Miller, Proc. R. Soc. A **463**, 1117 (2007).
[86] Y. Grabovsky and L. Truskinovsky, J. Nonlinear Sci. **23**, 891 (2013).
[87] P. Ciarletta and L. Truskinovsky, Phys. Rev. Lett. **122**, 248001 (2019).
[88] S. S. Pandurangi, A. Akerson, R. S. Elliott, T. J. Healey, and N. Triantafyllidis, J. Mech. Phys. Solids **160**, 104749 (2022).